

# Optical Manipulation of Microparticles in an SU-8/PDMS Hybrid Microfluidic Chip Incorporating a Monolithically Integrated On-Chip Lens Set

Honglei Guo, *Student Member, IEEE*, Ping Zhao, Gaozhi Xiao, *Member, IEEE*, Zhiyi Zhang, and Jianping Yao, *Senior Member, IEEE*

**Abstract**—An SU-8/PDMS microfluidic chip incorporating a monolithically integrated on-chip lens set for transport and manipulation of microparticles is developed. The components, including the on-chip lens set, the microfluidic channel, and the fiber grooves, are defined in a single layer of SU-8 by one-step photolithography. The design of the on-chip lens set and the fabrication of the microfluidic chip are fully described. The influence of the beam-waist radius on the manipulation performance is theoretically analyzed and experimentally verified for the first time. In the cross-type optofluidic architecture, the evaluation is performed by measuring the particle displacement with different beam-waist radii under different fluid-flow rates. The on-chip lens set is designed to have a specific dimension to achieve the required beam-waist radius. It is revealed that the particle displacement is counter-proportional to the beam-waist radius. An experiment is performed. The results show that the particle displacement is increased by reducing the beam-waist radius. The optical manipulation of microparticles is also demonstrated by using two counter-propagating light beams that are perpendicular to the fluid-flow direction with the beam-waist radius determined by two on-chip lens sets placed on the two sides of the microfluidic channel. The proposed architecture could be used to enhance the performance in particle transport, separation, and concentration.

**Index Terms**—Integrated devices, microfluidic device, optical manipulation.

## I. INTRODUCTION

THE POTENTIAL of integrating photonic and microfluidic elements into a “lab-on-a-chip” system or a miniaturized total analysis system ( $\mu$ TAS) has opened new routes to improve the performance of the particle transport and manipulation [1], [2]. These systems can be accomplished by various methods [3]. The well-known optical tweezer, achieved by using a tightly focused light beam, has already been proven to be a valuable research tool in the fields of biomanipulation [4] and flow cytometry [5]. However, this technique is restricted by the very short focal depth and the large light beam diffraction, which limit its capability in continuously transporting particles

and its overall strength in trapping particles [6]. To overcome these drawbacks, a range of near-field methods have recently been demonstrated by using planar optical waveguide [7], high-magnification total internal reflection (TIR) microscope objective [8], and subwavelength slot waveguides [6]. Although the use of the near-field methods would improve the transport and manipulation performance, the technique has limitations in two aspects. First, the very shallow penetration depth limits the height of the microfluidic channel [9]. Second, the waveguide structure has to be properly designed and fabricated to avoid the multimode distribution in the core waveguide [10]. The technique of optical chromatography is then developed to overcome these limitations. The first type of optical chromatography technique is defined as axial-type optical chromatography [11], where the scattering force resulted from the optical radiation and the fluid-drag force act on the particles in the opposite direction. Due to the sensitivity of the scattering force to the particle size and refractive index, this technique has been successfully applied to particle separation [12] and concentration [13]. The architecture has also been extended by using a core waveguide [14] and a hollow-core waveguide [15]. Fundamentally, however, the axial-type optical chromatography is not capable of continuously manipulating particles and requires additional devices to deliver the target particles out of the control region. A more recent cross-type optical chromatography technique is developed [16] as a solution to the problems, in which the light beam propagation is perpendicular to the fluid-flow direction. This orthogonal arrangement can manipulate particles in a continuous manner without the need of additional devices to move the target particles away [17]. Similar to other methods, the manipulation performance is highly dependent on the particle size and the refractive index, which have been fully described in [18] and [19]. On the other hand, the manipulation performance of the orthogonal arrangement also relies on the light-beam-waist radius at the microfluidic channel.

All microfluidic chips can be generally classified into two categories based on the materials used for the fabrication of the chips: the optical-planar-waveguide-based architectures and the poly-dimethylsiloxane (PDMS)-based architectures. Optical-planar-waveguide-based architectures can be fabricated by using the thin-film deposition or the anisotropic etching technique, which usually requires two or four photolithographic steps, with a procedure usually lasting up to a couple of weeks [20]. The fabrication process can be simplified by using the polymeric material [21], such as the SU-8 (negative photoresist). The use

Manuscript received August 1, 2009; revised September 5, 2009; accepted September 20, 2009. Date of publication December 1, 2009; date of current version August 6, 2010. This work was supported in part by the Centre for Photonics Fabrication Research and in part by The National Research Council, Canada.

H. Guo and J. Yao are with the Microwave Photonics Research Laboratory, School of Information Technology and Engineering, University of Ottawa, Ottawa, ON K1N 6N5, Canada (e-mail: jpyao@site.uottawa.ca).

P. Zhao, G. Xiao, and Z. Zhang are with the Institute for Microstructural Sciences, National Research Council Canada, Ottawa, ON K1A 0R6, Canada.

Color versions of one or more of the figures in this paper are available online at <http://ieeexplore.ieee.org>.

Digital Object Identifier 10.1109/JSTQE.2009.2033212

of PDMS-based architectures can also significantly reduce the complexity in the chip fabrication. However, a duration of at least 2 days is required to finish the steps of master-mold fabrication and the PDMS molding [22]. In addition, the incorporation of other optical elements, such as an on-chip lens, into the PDMS-based architectures will lead to the undesirable fabrication interactions. Especially, a high risk of distorting the optical elements during the processes of peering off the PDMS layer from the master mold and bonding it on the substrate would be resulted due to the microfeatures of the chip. In developing the “lab-on-a-chip” or  $\mu$ TAS system, the ability to fabricate a microfluidic chip in a fast manner with low complexity is highly desirable.

In this paper, we demonstrate a novel microfluidic chip with an improved particle transport and manipulation performance by incorporating a monolithically integrated on-chip lens set or a few on-chip lens sets in the microfluidic chip. The fundamental principle in the performance improvement is the reduction of the beam-waist radius by the on-chip lens set. A theoretical analysis of the operation, the design of the on-chip lens set, and the fabrication of the proposed SU-8/PDMS hybrid microfluidic chip are fully described in this paper. Especially, the influence of the light-beam-waist radius on the manipulation performance in a cross-type optofluidic architecture is discussed for the first time. Starting from the particle velocity (which is different from [16]), we obtain an analytical expression of the particle displacement induced by an ideal cross-type optically driven propulsion where the flow rate is assumed to have a constant value instead of a parabolic profile. The design of the on-chip lens set is then discussed and the modification of the light-beam-waist radius is demonstrated. The fabrication of the chip is also discussed in detail. Since the on-chip lens set, the microfluidic channel, and the fiber grooves are all defined in the same SU-8 layer, the chip fabrication and packaging are greatly simplified with a much shorter processing time.

## II. THEORY

The radiation forces applied to a particle resulted from the momentum transfer between the photon and the particle could be classified into two categories: the gradient force and the scattering force. The gradient force drives the particle to the center of the light beam, and eventually, retains all the particles at the focal point of the light beam. The scattering force drives the particle in the light-beam propagation direction. Given the assumption that the particle size is smaller than the light beam size, the gradient force is small and could be ignored. Therefore, the dominant force is the scattering force.

Based on the ray optics model [23] and the equation for the calculation of the scattering force [17], the particle displacement from the fluid-flow direction can be analytically derived from the particle velocity. Fig. 1 is a simplified illustration of the particle deflection, which is used to perform our analysis.

Assuming the light beam has an energy distribution of a Gaussian profile, the scattering force at position  $z$  is given by

$$F(z) = \frac{2nP}{c} \left( \frac{r_p}{\omega_0} \right)^2 Q \exp\left(-\frac{2z^2}{\omega_0^2}\right) \quad (1)$$

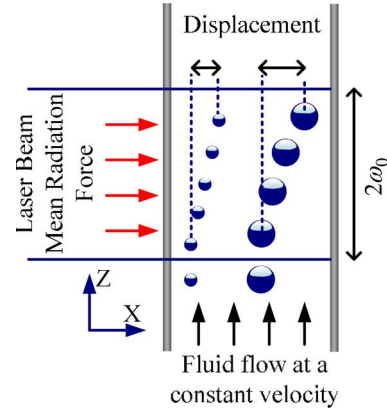


Fig. 1. Schematic of the optically driven transport.

where  $P$  is the power of the light beam,  $\omega_0$  is the light-beam-waist radius,  $r_p$  is the particle radius,  $n$  is the refractive index of the surrounding medium,  $Q$  is a dimensionless factor that is dependent on the refractive indices of both the particle and the surrounding medium, and  $z$  is the distance between the center of the particle and the light beam axis.

The mean value of the scattering force is obtained by integrating (1) within the light beam region, which is given by

$$F_M = \frac{1}{2\omega_0} \int_{-\omega_0}^{\omega_0} F(z) dz. \quad (2)$$

Substituting (1) into (2), we have

$$F_M = \sqrt{\frac{\pi}{2}} \operatorname{erf}(\sqrt{2}) \frac{nP}{c} \left( \frac{r_p}{\omega_0} \right)^2 Q \quad (3)$$

where  $\operatorname{erf}(\bullet)$  represents the error function resulted from the integration of the Gaussian function.

As shown in Fig. 1, the particles are flowing upward into the light beam region, from  $-\omega_0$  to  $\omega_0$  along the  $z$ -direction. When the particle reaches the light beam region, it is driven along the light beam axis by the force described in (3), which gives the particle a velocity along the  $x$ -direction, denoted as  $V_p$ . If we only consider the  $x$ -directional components of the vectors, such as the velocity and forces, the equation representing the particle motion in the  $x$ -direction can be written as

$$m_p \frac{dV_p}{dt} = F_M - F_D. \quad (4)$$

According to Stokes's law, the drag force, denoted as  $F_D$ , applied to the particle moving at a velocity of  $V_p$  is given by

$$F_D = 6\pi\eta r_p V_p \quad (5)$$

where  $\eta$  is the viscosity of the surrounding medium. Substituting (5) into (4), the particle velocity along the  $x$ -direction is given by [24]

$$V_p = \frac{F_M}{3\pi r_p \eta} (1 - e^{-t/\tau_p}) \quad (6)$$

where  $\tau_p$  is the particle relaxation time and its value is in the order of  $10^{-9}$  s. Since it is relatively small, the term  $e^{-t/\tau_p}$  in (6) can be neglected. Thus, the maximum particle velocity along

the  $x$ -direction can be obtained by

$$V_{pM} = \lim_{\tau_p \rightarrow 0} V_p = \frac{F_M}{3\pi r_p \eta}. \quad (7)$$

Considering that the initial particle velocity along the  $x$ -direction is zero, the displacement along the  $x$ -direction can be calculated as

$$x = \frac{1}{2} V_{pM} T \quad (8)$$

where  $T$  represents the time period within which the particle travels through the light beam region from  $-\omega_0$  to  $\omega_0$  at the  $z$ -directional velocity of  $U$ , which is regarded as the fluid-flow rate. As a pressure-driven fluid, the flow rate has a parabolic profile within the microfluidic channel, where the fluid that is closer to the microfluidic channel wall has a lower flow rate. The nonuniform flow-rate distribution is due to the viscous force between the fluid and the microfluidic channel [25]. In this paper, the theoretical model is set up for validating the proposed theory, that is, the particle displacement could be increased by reducing the light-beam-waist radius. In addition, surface treatment is applied to the microfluidic channel to reduce the viscous force between the fluid and the microfluidic channel, which could be used to keep the flow rate, to some extent, constant rather than having a parabolic profile. Thus, for the sake of simplicity, we assume that the fluid-flow rate is a constant value within the area where the particles are deflected by the incoming light beams. Therefore, for a time period  $T = 2\omega_0/U$ , substituting (3) and (7) into (8), we obtain the displacement as given by

$$x = \sqrt{\frac{\pi}{2}} \operatorname{erf}(\sqrt{2}) \frac{nP}{3\pi\eta U c \omega_0} \frac{r_p}{Q}. \quad (9)$$

It is seen that the displacement is counter-proportional to the light-beam-waist radius at the microfluidic channel. This conclusion is important since we can increase the displacement by using an on-chip lens set to reduce the waist radius rather than increasing the input light power.

### III. DESIGN AND FABRICATION

The key significance of the present paper is the incorporation of a monolithically integrated on-chip lens set into a microfluidic chip, by which the beam-waist radius is reduced, which leads to an improved performance in the optofluidic transport and optical manipulation. An on-chip lens [26] is originally designed to enhance the detection efficiency of a scattered light [27], [28]. In this section, the design of an on-chip lens set is described, and the use of an on-chip lens set to reduce the beam-waist radius is demonstrated. The chip fabrication is also detailed in this section. The schematic of a microfluidic chip is shown in Fig. 2.

As illustrated in Fig. 2, two on-chip lenses (such as On-Chip Lens 1 and On-Chip Lens 2) are used to form an on-chip lens set (such as On-Chip Lens Set 2) to achieve a specific light-beam-waist radius. On the right side of the microfluidic channel, three sets of lenses with different lens dimensions are fabricated

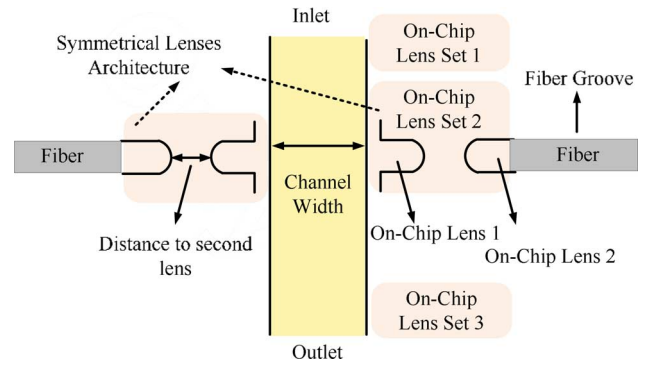


Fig. 2. Schematic of a microfluidic chip incorporating on-chip lens sets.

TABLE I  
DIMENSIONS OF ON-CHIP LENS SET 2 STRUCTURE<sup>a</sup>

Lens 1	Curvature	-300
	Aperture radius	500
	Distance to second lens	300
Lens 2	Curvature	190
	Aperture radius	500

<sup>a</sup>The unit is micrometer ( $\mu\text{m}$ ).

<sup>b</sup>Negative curvature means a concave lens, while positive curvature means a convex lens.

and placed along the channel, as shown in Fig. 2. These three different light-beam-waist radii can be achieved by the on-chip lens sets. The lens dimension settings for On-Chip Lens Set 2, illustrated in Fig. 2, are listed in Table I.

In order to achieve the optical manipulation by using two counter-propagating light beams, a symmetric architecture by incorporating on-chip lens sets on the other side of the microfluidic channel is designed, which is denoted as ‘‘Symmetrical Lenses Architecture’’ in Fig. 2.

The width of the microfluidic channel is designed to be  $100 \mu\text{m}$  and the height is  $130 \mu\text{m}$ , which are determined by the size of the external optical fiber. The fiber used in this paper has a core radius of  $52.5 \mu\text{m}$  and a cladding radius of  $60 \mu\text{m}$ . The input light beam is introduced into the on-chip lens by butt coupling. The fiber groove is used to fix the fiber, which avoids the use of a high-precision positioning stage and simplifies the alignment.

In On-Chip Lens Set 2, for example, we show the overall field view of the fiber groove and the lens structure in both bright and dark fields in Fig. 3.

All the three on-chip lens sets are shown in Fig. 4(a), and the resulted light beams with different waist radii on the microfluidic channel are shown in Fig. 4(b). The light-beam-waist radius on the microfluidic channel can be estimated in each on-chip lens set with the assistance of the known channel width, which is fixed at  $100 \mu\text{m}$  (defined by the photomask). By comparing the distance of the channel width and light-beam-waist radius obtained from Fig. 4(b), the light-beam-waist radii are measured to be  $\sim 75$ ,  $\sim 50$ , and  $\sim 100 \mu\text{m}$  (total light beam sizes of  $\sim 150$ ,  $\sim 100$ , and  $\sim 200 \mu\text{m}$ ) for On-Chip Lens Sets 1, 2, and 3, respectively.

The architecture of the proposed microfluidic chip is illustrated in Fig. 5. It is fabricated with the photolithography

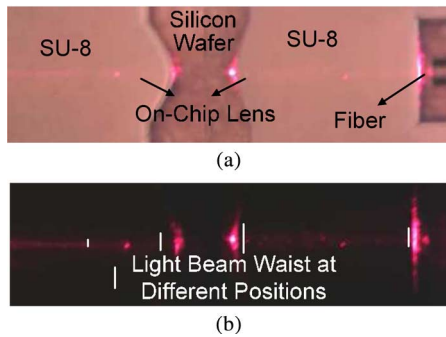


Fig. 3. Microscopic images of On-Chip Lens Set 2 (the microfluidic channel is on the left side of the images and is not shown here due to the limited imaging field). (a) Bright-field image. (b) Dark-field image with the incident light beam of He-Ne laser (632.8 nm, 20 mW).

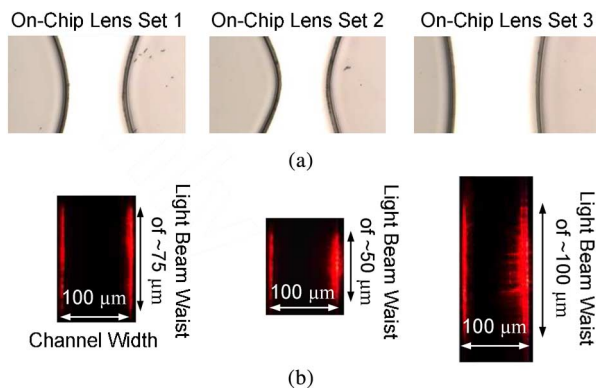


Fig. 4. (a) Illustration of the three on-chip lens structures. (b) Light beam waist on the microfluidic channel. (a) and (b) are not in the same scale.

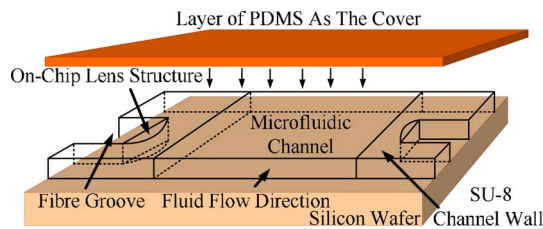


Fig. 5. Illustration of the proposed microfluidic chip architecture.

technique [29]. In general, the on-chip lens set, the microfluidic channel, and the fiber grooves are defined in the same layer of SU-8 (SU-8 2075, MicroChem). All these components are fabricated based on a 4-in silicon wafer as the substrate. The use of a silicon wafer makes it simple to fabricate the 130- $\mu\text{m}$ -thick architecture. During the fabrication process, the silicon wafer is first cleaned in a "Piranha" solution ( $\text{H}_2\text{O}_2:\text{H}_2\text{SO}_4 = 1:4$ ) for 30 min, and is then thoroughly washed by distilled water, followed by a dehydration process in a 250 °C oven for 3 h to improve the adhesion of the SU-8. The 130- $\mu\text{m}$ -thick SU-8 layer is spun onto the wafer with a rotation speed of 1500 r/min after the wafer is cooled down to the room temperature. The microstructures are defined on the SU-8 layer by UV photolithography. The post-exposure bake is implemented by putting the microfluidic chip on a hotplate with the temperature of the hotplate being increased to 100 °C at a temperature ramp of 10 °C/min, and then keeping

the temperature at 100 °C for 30 min. The microfluidic chip is then further cooled down to the room temperature. The microfluidic chip is developed in the SU-8 developer for 30 min. Finally, our newly home-developed bonding technique [30] is employed to apply a layer of premade PDMS on top of the SU-8 based microstructures as a cover. Our home-developed bonding technique makes the whole fabrication process easier to handle compared with the technique applying spring-mounted screws reported in [27]. Since only one mask is required in the fabrication process and the architecture is fabricated on SU-8, the proposed SU-8/PDMS hybrid microfluidic chip can be made, packaged, and tested in a single fabrication step, which would significantly reduce the processing time to one day compared with other existing methods where a relatively long processing time of a few days is usually needed. In addition, the fabrication complexity is also significantly reduced.

After the SU-8/PDMS microfluidic chip is fabricated, surface treatment should be applied to the microfluidic channel for two reasons [31]. First, surface treatment is used to reduce the viscous force between the fluid and the microfluidic channel to make the flow rate, to some extent, constant within the channel rather than having a parabolic profile. Second, surface treatment can prevent the samples (microparticles) from attaching on the microfluidic channel. Surface treatment is implemented first by introducing 3% Pluronic F68 into the channel. Then, the channel is rinsed with phosphate buffered saline (PBS) to remove any residue of Pluronic F68 before introducing any sample.

#### IV. EXPERIMENTAL RESULTS AND DISCUSSION

Polystyrene particles (Polystyrene Microsphere, refractive index of 1.59, Polysciences) are used in this paper to evaluate the performance of the developed microfluidic chip for microparticle transport and manipulation. The radii of the polystyrene particles are 1 and 3  $\mu\text{m}$ . The particles are first diluted to a concentration of  $10^5$  samples/mL, and then introduced into the microfluidic chip with a 1-mL syringe and a syringe pump (Pump 33, Harvard apparatus).

A continuous-wave fiber laser (Custom designed, fiber tail of AFS 105/125Y, NA = 0.22, WT&T) with an operating wavelength of 1064 nm and an output power of 0.5 W is employed to provide the input light beam. The motions of the particles are captured using an imaging system that consists of a microscope (Nikon, Inc.), a 20 $\times$ -microscope objective (Infinity-Corrected long working distance objective, Mitutoyo), and a charge-coupled device (CCD) camera (Infinity 2-2, Lumenera).

The performance of the optofluidic transport is evaluated by measuring the particle displacements. A light beam with a beam-waist radius of 50, 75, or 100  $\mu\text{m}$ , achieved using one of the three on-chip lens sets, is applied to perform the measurement. Although the light beam is loosely focused by the on-chip lens set, the light-beam-waist radius is still larger than the particle radius. Therefore, the assumption that the gradient force is negligible and the scattering force is the dominant radiation force is still valid.

The optofluidic transport of microparticles with a radius of 3  $\mu\text{m}$  is first performed. Experimental results are shown in

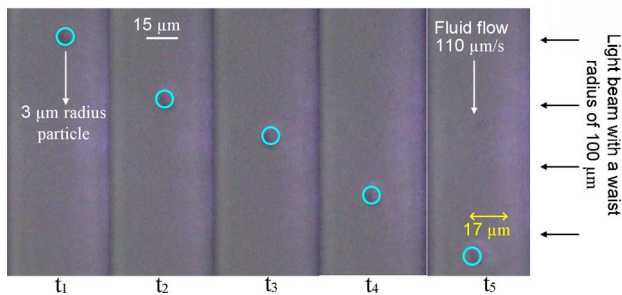


Fig. 6. Snapshots of the transport of a 3- $\mu\text{m}$ -radius particle with the light-beam-waist radius of 100  $\mu\text{m}$  at a flow rate of 110  $\mu\text{m}/\text{s}$ . The cropping location is the same in each time-lapse image.

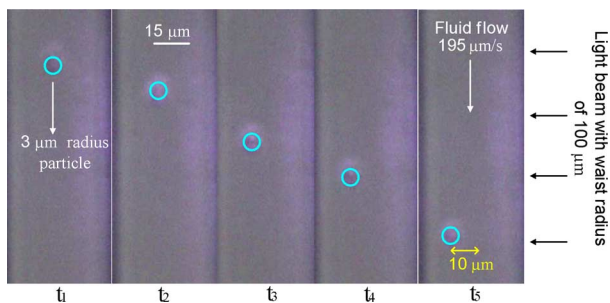


Fig. 7. Snapshots of the transport of a 3- $\mu\text{m}$ -radius particle with the light-beam-waist radius of 100  $\mu\text{m}$  at a flow rate of 195  $\mu\text{m}/\text{s}$ . The cropping location is the same in each time-lapse image.

Figs. 6 and 7, where the flow rates are 110 and 195  $\mu\text{m}/\text{s}$ , respectively.

The fluid flows downward in the microfluidic channel, and the input light beam with a modified waist radius of 100  $\mu\text{m}$  is introduced into the microfluidic channel from the right to the left, which drives the particle to the left direction. This orthogonal arrangement is defined as the cross-type optofluidic transport as discussed earlier. A series of snapshots obtained at different instants, starting from  $t_1$  to  $t_5$ , are shown. It is seen that the 3- $\mu\text{m}$ -radius particles have been driven with different displacement at different flow rates.

Particle displacements are also measured with the other two light-beam-waist radii at different flow rates. A comparison between the theoretical and experimental results is shown in Fig. 8.

In Fig. 8, the particle displacement is evaluated as a function of the light-beam-waist radius and the flow rate. In all cases, the measured displacements agree well with the theoretical predictions. As can be seen, the displacement is increased by reducing the light-beam-waist radius. This conclusion is important since it provides a potential solution to enhance the performance of a microfluidic chip for the optofluidic transport and optical manipulation by defining its architecture rather than using a high-power laser. It is also seen that a small deviation exists between the measured and theoretical displacements, which is believed to be resulted mainly from the assumption that the fluid-flow rate keeps constant within the microfluidic channel, whereas it should have a parabolic profile as discussed in Section II. However, as can be seen from Fig. 8, it is deemed sufficient

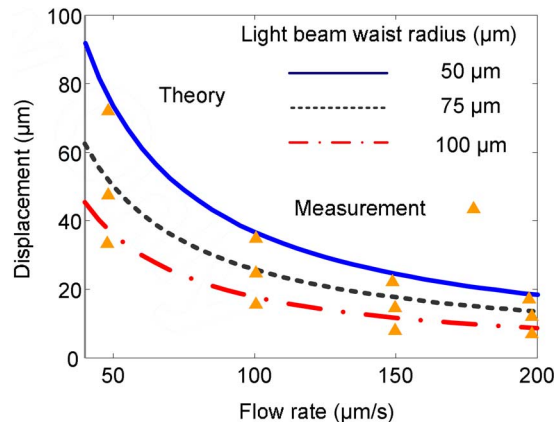


Fig. 8. Measured and simulated displacements as a function of the flow rate and the light-beam-waist radius. The comparison is made for a microparticle with a 3- $\mu\text{m}$  radius.

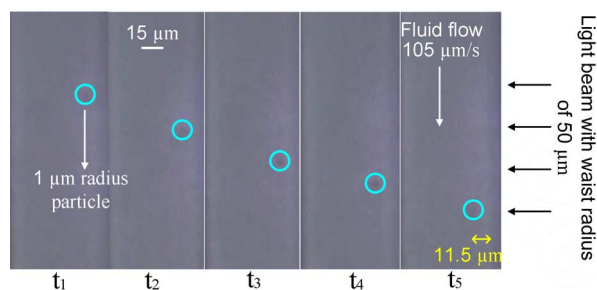


Fig. 9. Snapshots of the transport of a 1- $\mu\text{m}$ -radius particle with the light-beam-waist radius of 50  $\mu\text{m}$  at a flow rate of 105  $\mu\text{m}/\text{s}$ . The cropping location is the same in each time-lapse image.

for the purpose of demonstrating that the displacement could be enhanced by reducing the light-beam-waist radius.

Then, the optofluidic transport of the 1- $\mu\text{m}$ -radius particles is experimented. Fig. 9 shows the experimental result, which is obtained using a light beam with a waist radius of 50  $\mu\text{m}$ , and the particles are moving at a flow rate of 105  $\mu\text{m}/\text{s}$ . A comparison between the experimental and theoretical displacements of the 1- $\mu\text{m}$ -radius particle is shown in Fig. 10. Again, a reduced waist radius leads to an increased displacement in the optofluidic transport.

Third, the optofluidic transport of mixed particles with two different radii is experimented. The experimental results are shown in Fig. 11. Again, the measured displacements of the particles with different radii agree well with the theoretical predictions, as shown in Figs. 8 and 10. If we compare the displacements of the particles with different radii, we will find that the displacement of the 3- $\mu\text{m}$ -radius particle is three times that of the 1- $\mu\text{m}$ -radius particle, which confirms the relationship between the particle size and the displacement, as shown in (9).

Finally, the optical manipulation of a 3- $\mu\text{m}$ -radius particle is demonstrated using the developed microfluidic chip. The motion of the particle is controlled by two counter-propagating light beams introduced into the microfluidic chip from two opposite sides, both propagating perpendicularly to the fluid-flow direction. The second light beam is provided by a fiber laser source (Custom designed, standard single-mode fiber, WT&T)

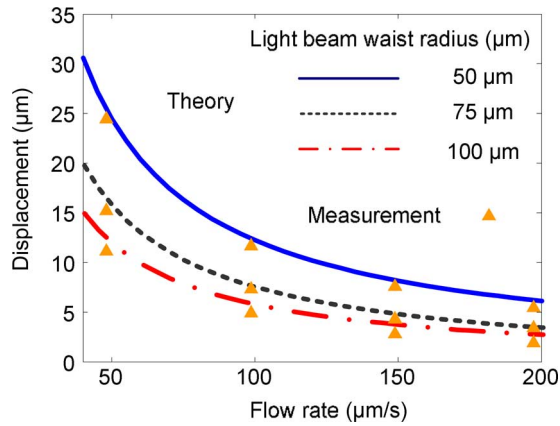


Fig. 10. Measured and simulated displacements as a function of the flow rate and light-beam-waist radius. The comparison is made for a microparticle with a  $3\text{-}\mu\text{m}$  radius.

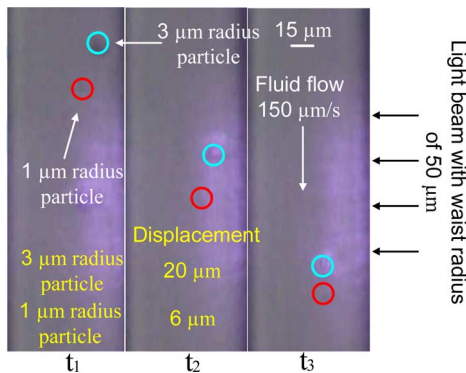


Fig. 11. Snapshots of the transport of mixed particles of radii 1 and  $3\text{ }\mu\text{m}$ , respectively, with the light-beam-waist radius of  $50\text{ }\mu\text{m}$  at a flow rate of  $150\text{ }\mu\text{m/s}$ . The cropping location is the same in each time-lapse image.

with an operating wavelength of  $1067\text{ nm}$  and an output power of  $150\text{ mW}$ . The two output fibers of the two laser sources are fixed in the fiber grooves on each side of the microfluidic channel, as shown in Fig. 5. On-Chip Lens Set 2, as shown in Fig. 2, is used to achieve a light-beam-waist radius of  $50\text{ }\mu\text{m}$ , and another on-chip lens set on the opposite side is used to achieve a light-beam-waist radius of  $10\text{ }\mu\text{m}$ . The use of the two counter-propagating light beams is different from the optical trapping reported in [32], where a pair of single-mode fibers or a pair of multimode fibers was used to achieve the optical trapping. However, in this paper, the optical manipulation of a microparticle is performed by the optofluidic transport, which is different from the optical trapping. In addition, the optical manipulation ability is important for the assembly techniques and optically driven bioanalytics [33]. Furthermore, the analysis of the mode distribution in the cross section of the two light beams and the precise control of their output power, as required for the optical trapping in [32], are not necessarily considered in the proposed optical manipulation scheme, because we are only considering the mean value of the radiation forces, as illustrated in (2). Therefore, it is a simple process to achieve optical manipulation.

The optical manipulation is shown in Fig. 12 with six steps from Fig. 12(a) to (f). Fig. 12(a) shows the area of the control

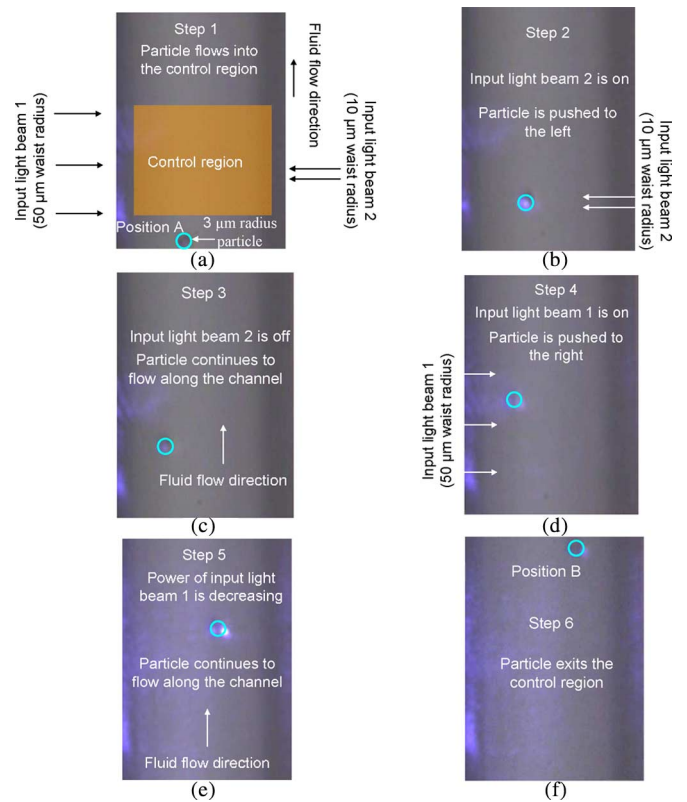


Fig. 12. Optical manipulation of a  $3\text{-}\mu\text{m}$ -radius particle by controlling the powers of the two light beams.

region. At the beginning, the two lasers are off. After the particle flows into the control region at Position A, Laser 2 is switched on, and input light beam 2 drives the particle to the left, as shown in Fig. 12(b). After the particle has been driven with a displacement to the left direction, Laser 2 is off and the particle continues to flow along the microfluidic channel, as shown in Fig. 12(c). Then, Laser 1 is turned on and input light beam 1 pushes the particle to the right, as shown in Fig. 12(d). When the particle reaches a position as shown in Fig. 12(e), Laser 1 is turned off. The particle then leaves the control region at Position B, as shown in Fig. 12(f).

It is seen that the output position and the moving path inside the control region can be defined by the two lasers. The architecture for the manipulation of the particle shown in Fig. 12 can be considered as an optical manipulation unit. By placing a number of these units along the microfluidic channel, the transport of a particle to a specific position can be accomplished. With the modified waist radius of the input light beams, the optofluidic transport performance can be maximized in each unit. This will improve the performance of the optical manipulation. In addition, a further expected performance for this device is that the particle displacement could be further increased to over  $200\text{ }\mu\text{m}$  by designing a compound on-chip lens structure while keeping a low power of the input light beam. For this displacement, we believe it is sufficient to separate the target particles. In such a case, the proposed SU-8/PDMS microfluidic chip with a monolithically integrated compound on-chip lens structure is expected to be applied for applications in optofluidic sorting and

switching [34], with the particle manipulation capability demonstrated in Fig. 12.

## V. CONCLUSION

An SU-8/PDMS microfluidic chip incorporating a monolithically integrated on-chip lens for the transport and manipulation of microparticles was developed and experimentally demonstrated. The design of the on-chip lens sets and the fabrication of the microfluidic chip were fully described. The dependence of the optofluidic transport on the light-beam-waist radius using an on-chip lens set was evaluated for the first time. It was shown that an increased particle displacement was achieved with a reduced light-beam-waist radius. The displacements of particles with different radii under different flow rates were also measured. The experimental results agreed well with the theoretical analysis. In addition to the transport of a microparticle using the developed microfluidic chip, the use of the microfluidic chip for the optical manipulation of a particle was also demonstrated, which was achieved by introducing two counter-propagating light beams into the microfluidic chip using two on-chip lens sets placed on the two sides of the microfluidic channel. The incorporation of multiple on-chip lens structures with the compound lens design in the microfluidic chip would make the proposed microfluidic chip to have an improved functionality for the transport and manipulation of microparticles for different optofluidic sorting and switching applications.

## REFERENCES

- [1] D. Psaltis, S. R. Quake, and C. H. Yang, "Developing optofluidic technology through the fusion of microfluidics and optics," *Nature*, vol. 442, pp. 381–386, Jul. 2006.
- [2] C. Monat, P. Domachuk, and B. J. Eggleton, "Integrated optofluidics: A new river of light," *Nature Photon.*, vol. 1, pp. 106–114, Feb. 2007.
- [3] H. Andersson and A. Van Den Berg, "Microfluidic devices for cellomics: A review," *Sens. Actuators B*, vol. 92, no. 3, pp. 315–325, May 2003.
- [4] C. L. Kuyper and D. T. Chiu, "Optical trapping: A versatile technique for biomanipulation," *Appl. Spectrosc.*, vol. 56, no. 11, pp. 300A–321A, Feb. 2002.
- [5] M. M. Wang, "Microfluidic sorting of mammalian cells by optical force switching," *Nature Biotechnol.*, vol. 23, no. 1, pp. 83–87, Dec. 2005.
- [6] A. H. J. Yang, S. D. Moore, B. S. Schmidt, M. Klug, M. Lipson, and D. Erickson, "Optical manipulation of nanoparticles and biomolecules in sub-wavelength slot waveguides," *Nature*, vol. 457, pp. 71–75, Jan. 2009.
- [7] K. Grujic and O. G. Helleso, "Dielectric microsphere manipulation and chain assembly by counter-propagating waves in a channel waveguide," *Opt. Exp.*, vol. 15, no. 10, pp. 6470–6477, May 2007.
- [8] R. F. Marchington, M. Mazilu, S. Kuriakose, V. Garces-Chavez, P. J. Reece, T. F. Krauss, M. Gu, and K. Dholakia, "Optical detection and sorting of microparticles in a near-field optical geometry," *Opt. Exp.*, vol. 16, no. 6, pp. 3712–3726, Mar. 2008.
- [9] K. Grujic and O. G. Helleso, "Dielectric microsphere manipulation and chain assembly by counter-propagating waves in a channel waveguide," *Opt. Exp.*, vol. 15, no. 10, pp. 6470–6477, May 2007.
- [10] T. Tanaka and S. Yamamoto, "Optically induced propulsion of small particles in an evanescent field of higher propagation mode in a multimode, channelled waveguide," *Appl. Phys. Lett.*, vol. 77, no. 20, pp. 3131–3133, Nov. 2000.
- [11] T. Kaneta, Y. Ishidze, N. Mishima, and T. Imasaka, "Theory of optical chromatography," *Anal. Chem.*, vol. 69, no. 14, pp. 2701–2310, Jul. 1997.
- [12] S. J. Hart and A. V. Terray, "Refractive-index-driven separation of colloidal polymer particles using optical chromatography," *Appl. Phys. Lett.*, vol. 83, no. 25, pp. 5316–5318, Dec. 2003.
- [13] S. J. Hart, A. V. Terray, J. Arnold, and T. A. Leski, "Sample concentration using optical chromatography," *Opt. Exp.*, vol. 15, no. 5, pp. 2724–2731, Mar. 2007.
- [14] S. Mandal and D. Erickson, "Optofluidic transport in liquid core waveguiding structures," *Appl. Phys. Lett.*, vol. 90, pp. 184103.1–1841063.3, May 2007.
- [15] P. Measor, S. Kuhn, E. J. Lunt, B. S. Phillips, A. R. Hawkins, and H. Schmidt, "Hollow-core waveguide characterization by optically induced particle transport," *Opt. Lett.*, vol. 33, no. 7, pp. 672–674, Apr. 2008.
- [16] S. B. Kim, J. H. Kim, and S. S. Kim, "Theoretical development of in situ optical particle separator: Cross-type chromatography," *Appl. Opt.*, vol. 45, no. 27, pp. 6919–6924, Sep. 2006.
- [17] S. B. Kim, S. Y. Yoon, H. J. Sung, and S. S. Kim, "Cross-type optical particle separation in a microchannel," *Anal. Chem.*, vol. 80, no. 7, pp. 2628–2630, Feb. 2008.
- [18] S. B. Kim, S. Y. Yoon, H. J. Sung, and S. S. Kim, "Resolution of cross-type optical particle separation," *Anal. Chem.*, vol. 80, no. 15, pp. 6023–6028, Jul. 2008.
- [19] S. B. Kim, E. J. H. J. Sung, and S. S. Kim, "Optical mobility in cross-type optical particle separation," *Appl. Phys. Lett.*, vol. 93, pp. 044103.1–044103.3, Aug. 2008.
- [20] K. B. Mogensen, Y. C. Kwok, J. C. Eijkel, N. J. Peterson, A. Manz, and J. P. Kutter, "A microfluidic device with an integrated waveguide beam splitter for velocity measurements of flowing particles by Fourier transformation," *Anal. Chem.*, vol. 75, no. 18, pp. 4931–4936, Aug. 2003.
- [21] L. Eldada and L. W. Shacklette, "Advances in polymer integrated optics," *IEEE J. Sel. Topics Quantum Electron.*, vol. 6, no. 1, pp. 54–68, Jan./Feb. 2000.
- [22] D. A. Chang-Yen, R. K. Eich, and B. K. Gale, "A monolithic PDMS waveguide system fabricated using soft-lithography techniques," *J. Lightw. Technol.*, vol. 23, no. 6, pp. 2088–2093, Jun. 2005.
- [23] A. Ashkin, "Forces of a single-beam gradient laser trap on a dielectric sphere in the ray optics regime," *Biophys. J.*, vol. 61, no. 2, pp. 569–582, Feb. 1992.
- [24] W. C. Hinds, *Aerosol Technology: Properties, Behavior, and Measurement of Airborne Particles*. New York: Wiley-Interscience, 1999.
- [25] W. C. Tian and E. Finehout, *Microfluidics for Biological Applications*. New York: Springer-Verlag, 2008, ch. 1.
- [26] S. Camou, H. Fujita, and T. Fujii, "PDMS 2D optical lens integrated with microfluidic channels: Principle and characterization," *Lab Chip*, vol. 3, no. 1, pp. 40–45, Feb. 2003.
- [27] Z. Wang, J. El-Ali, M. Englund, T. Gotaed, I. R. Perch-Nielsen, K. B. Mogensen, D. Snakenborg, J. P. Kutter, and A. Wolff, "Measurements of scattered light on a microchip flow cytometer with integrated polymer based optical elements," *Lab Chip*, vol. 4, no. 4, pp. 372–377, Apr. 2004.
- [28] J. Seo and L. P. Lee, "Disposable integrated microfluidic with self-aligned planar microlenses," *Sens. Actuators B*, vol. 99, no. 2/3, pp. 615–622, Jan. 2004.
- [29] K. B. Mogensen, J. El-Ali, A. Wolff, and J. P. Kutter, "Integration of polymer waveguides for optical detection in microfabricated chemical analysis systems," *Appl. Opt.*, vol. 42, no. 19, pp. 4072–4079, Jul. 2003.
- [30] Z. Y. Zhang, P. Zhao, and G. Z. Xiao, "The fabrication of polymer microfluidic devices using a solid-to-solid interfacial polyaddition," *Polymer*, vol. 50, no. 23, pp. 5358–5361, Nov. 2009.
- [31] K. Boxshall, M.-H. Wu, Z. Cui, Z. F. Cui, J. F. Watts, and M. A. Baker, "Simple surface treatments to modify protein adsorption and cell attachment properties within a poly(dimethylsiloxane) micro-bioreactor," *Surf. Interface Anal.*, vol. 38, no. 4, pp. 198–201, Apr. 2006.
- [32] D. Rudd, C. Lopez-Mariscal, M. Summers, A. Shahvisi, J. C. Gutierrez-Vega, and D. McGloin, "Fiber based optical trapping of aerosols," *Opt. Exp.*, vol. 16, no. 19, pp. 14550–14560, Sep. 2008.
- [33] S. J. Hart, A. Terray, T. A. Leski, J. Arnold, and R. Stroud, "Discovery of a significant optical chromatographic difference between spores of *Bacillus anthracis* and its close relative, *Bacillus thuringiensis*," *Anal. Chem.*, vol. 78, no. 9, pp. 3221–3225, Mar. 2006.
- [34] C.-T. Ho, R. Z. Lin, H. Y. Chang, and C. H. Liu, "Micromachined electrochemical T-switches for cell sorting applications," *Lab Chip*, vol. 5, no. 12, pp. 1248–1258, Sep. 2005.

**Honglei Guo** (S'08) received the M.S. degree in optics from Nankai University, Tianjin, China, in 2006. He is currently working toward the Ph.D. degree with the Microwave Photonics Research Laboratory, School of Information Technology and Engineering, University of Ottawa, Ottawa, ON, Canada.

His research interests include fiber optic sensors, sensor interrogation systems, micro- and nano-photonics fabrication, biophotonics, and microwave photonics.

**Gaozhi Xiao** (M'05) received the Ph.D. degree in material engineering from Loughborough University of Technology, Leicestershire, U.K., in 1995.

He is currently a Research Officer in the Institute for Microstructural Sciences, National Research Council Canada, Ottawa, ON, Canada. His research interests include the development of microfiber optic sensor systems for aerospace applications and physical-chemical sensing applications.

**Zhiyi Zhang** received the Ph.D. degree in polymer science from Zhongshan University, Guangzhou, China, in 1990.

From 1990 to 2001, he was with Zhongshan University, Guangzhou, China, Loughborough University, Leicestershire, U.K., McMaster University, Hamilton, Canada, National Research Council Canada, Ottawa, ON, Canada, Woodbridge Group Company, Mississauga, Canada, and Zenastra Photonics, Inc., Ottawa. Since 2002, he has been a Research Officer with the Institute for Microstructural Sciences, NRC. His current research interests include microfluidics, photonic sensors, and photonic materials.



**Jianping Yao** (M'99–SM'01) received the Ph.D. degree in electrical engineering from the Université de Toulon, Toulon, France, in 1997.

Since 2001, he has been with the School of Information Technology and Engineering, University of Ottawa, Ottawa, ON, Canada, where he is currently a Professor and Director of the Microwave Photonics Research Laboratory, and Director of the Ottawa-Carleton Institute for Electrical and Computer Engineering, Ottawa. From 1999 to 2001, he was in the faculty with the School of Electrical and Electronic Engineering, Nanyang Technological University, Singapore. He is also a Yongqian Endowed Visiting Chair Professor with Zhejiang University, Hangzhou, China. He was an invited Professor for 3 months with the Institut National Polytechnique de Grenoble, Grenoble, France, in 2005. His research interests include microwave photonics, which includes all-optical microwave signal processing, photonic generation of microwave, mm-wave and THz, radio over fiber, UWB over fiber, fiber Bragg gratings for microwave photonics applications, and optically controlled phased-array antenna, fiber lasers, fiber-optic sensors, and biophotonics. He is the author or coauthor of more than 130 papers in refereed journals and 110 papers in conference proceeding.

Dr. Yao is a Member of International Society of Optical Engineering, a Fellow of Optical Society of America, and a Senior Member of IEEE Photonics Society and IEEE Microwave Theory and Techniques Society. He is an Associate Editor of the International Journal of Microwave and Optical Technology. He is a Registered Professional Engineer in the State of Ontario. He is on the Editorial Board of IEEE TRANSACTIONS ON MICROWAVE THEORY AND TECHNIQUES. He was the recipient of the 2005 International Creative Research Award of the University of Ottawa, the 2007 George S. Glinski Award for Excellence in Research, and a Natural Sciences and Engineering Research Council of Canada Discovery Accelerator Supplements award in 2008. He was named University Research Chair in Microwave Photonics in 2007.